NOTICE

CERTAIN DATA CONTAINED IN THIS DOCUMENT MAY BE DIFFICULT TO READ IN MICROFICHE PRODUCTS.

SAND--90-1978C

DE91 001341

1990

TUBULAR LAP JOINTS FOR WIND TURBINE APPLICATIONS: TEST AND ANALYSIS

E. D. Reedy, Jr. and T. R. Guess
Sandia National Laboratories
Albuquerque, New Mexico

ABSTRACT

A combined analytical/experimental study of the strength of thick-walled, adhesively bonded PMMA-to-aluminum and E-glass/epoxy composite-to-aluminum tubular lap joints under axial load has been conducted. Test results include strength and failure mode data. Moreover, strain gages placed along the length of the outer tubular adherend characterize load transfer from one adherend to the other. The strain gage data indicate that load transfer is nonuniform and that the relatively compliant PMMA has the shorter load transfer length. Strains determined by a finite element analysis of the tested joints are in excellent agreement with those measured. Calculated bond stresses are highest in the region of observed failure, and extensive bond yielding is predicted in the E-glass/epoxy composite-to-aluminum joint prior to joint failure.

INTRODUCTION

Many horizontal axis wind turbine (HAWT) blades now in use are made of an E-glass reinforced resin composite. Composite material blades are also being considered for use on vertical axis wind turbines (VAWTs). The strength and fatigue resistance of composite material blades are clearly of importance. Indeed, composite material blades are experiencing fatigue related failures that have significantly shortened their expected lifetime. Such failures often occur in the region of joints or other discontinuities.

A common design for a composite material wind turbine blade is a spar and shell. This type of design uses composite materials in an efficient manner, and can be used for both HAWT and VAWT blades. Typically, the blade attachment joint in a spar and shell design has a tubular geometry, with a thick, composite adherend joined to a metallic hub. A bonded, composite-to-metal tubular lap joint is perhaps the simplest joint design of this type.

Although there is an extensive published literature on lap joints between flat plates, there are few papers addressing tubular lap joints subjected to axial load. Lubkin and Reissner [1] present results of an approximate analysis for tubular lap joints with equal thickness, same material, isotropic adherends. The results of this study suggest that tubular lap joints behave in a qualitatively similar manner to flat plate lap joints, but the stress distribution in the two types of joints differ in detail. Accordingly, the stress distribution in a tubular lap joint cannot be related to that of a similar flat lap joint. In a more recent publication, Adams and Peppiatt [2] present results of finite element analyses of some of the configurations examined by Lubkin and Reissner. Their calculated stress distributions are in good agreement with those of Lubkin and Reissner except when very close to a bond end. Adams and Peppiatt also show that an adhesive fillet can affect calculated stress distributions. There appears to be little published literature on metal-to-composite tubular lap joints subjected to axial load. (Several papers examining a torsional loading of such joints have been found. These analyses are aimed at composite material drive shaft applications.)

Presented below are results of a combined analytical/experimental study of thick-walled, adhesively bonded PMMA-to-aluminum and E-glass/epoxy composite-to-aluminum tubular lap joints. Joints with an E-glass/epoxy adherend are of technological importance, while those with a PMMA (acrylic) adherend allow direct observation of joint failure. All tested joints were subjected to a monotonic tensile or compressive loading. Test results include strength and failure mode data and serve as a baseline for planned fatigue tests.

JOINT TEST SPECIMENS

The E-glass/epoxy composite-to-aluminum joint test specimen bonds an aluminum tube within each end of an E-glass/epoxy tube (Fig. 1). Note that the specimen is axisymmetric (the axis of symmetry is indicated by the dashed horizontal line in Fig. 1), and is also symmetric about its midplane (the midplane position is

indicated by the vertical centerline in Fig. 1). The outer E-glass/epoxy tubular adherend is roughly 300 mm long, with a 76.2 mm diameter and a 6.4 mm wall thickness (r/t~6). The aluminum adherends are 12.5 mm thick. The bond thickness between adherends is 0.25 mm, and the bond length is 75 mm. Note, the bond end located 75 mm from the end of the E-glass/epoxy tube (i.e. where the aluminum adherend terminates) will be referred to as the inner bond end. The E-glass/epoxy tubes were obtained from General Electric and are fabricated from a plain weave, glass fabric with 32 yarns/inch axial and 44 yarns/inch hoop. The PMMA-to-aluminum joint test specimens are similar to the E-glass/epoxy composite-to-aluminum specimens, except that the PMMA tubular adherend is roughly 270 mm long.

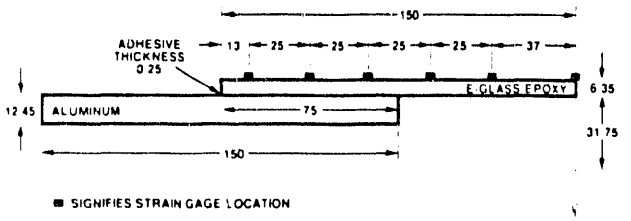

Fig. 1. E-glass/epoxy composite-to-aluminum joint test specimen.
All dimensions in mm.

The joint specimens were fabricated using a method that carefully controls bond line thickness and also minimizes voids within the bond. First the bond volume is defined and isolated using spacers and elastomeric dams, then the adhesive is injected into this cavity through four fill holes in the outer adherend. The fill holes are 90 degrees apart and are axially centered with respect to the 75 mm long bond. The bonding material is a room temperature cured, high strength paste adhesive (Hysol EA 9394). The efficacy of this procedure to produce void-free, uniform thickness bonds was confirmed by a visual inspection of those joints with a transparent PMMA outer adherend. Joints with an opaque E-glass/epoxy outer adherend were inspected ultrasonically using the C-scan technique. As an aside, PMMA-to-aluminum joints containing known voids were inspected using the C-scan method to verify that this technique could detect voided regions within a bond.

All joint test specimens were instrumented with strain gages. Strain gage locations on E-glass/epoxy composite-to-aluminum joints are shown in Fig. 1. There are a total of ten gages, all located on one end of the specimen. At the specimen's midplane, 150 mm from the end of the 300 mm long composite tube, there are 4 axial gages spaced at 90 degree intervals and one transverse gage. These midplane gages are in a uniformly stressed region that is undisturbed by the adhesive bond. Consequently, the outer adherend's axial modulus and Poisson's ratio can be directly measured. PMMA-to-aluminum joints were also instrumented with 10 strain gages. To accommodate the slightly shorter PMMA tube length, gage locations differ somewhat from those shown in Fig. 1 (axial gage locations are 25, 50, 75, 100, and 133 mm from the end of the PMMA adherend). The joint specimens were loaded monotonically to failure in a 450 kN mechanical testing machine. Universal joints were used on both ends of the load train, and the aluminum adherends were attached to the universal joints by threaded rods.

TEST RESULTS

Two PMMA-to-aluminum and two E-glass/epoxy composite-to-aluminum joints have been loaded monotonically to failure. Test results are summarized in Table 1. Here, the PMMA-to-aluminum tests will be referred to as PMMA-1 and PMMA-2, while the E-glass/epoxy composite-to-aluminum tests will be referred to as E/G-1 and E/G-2. Also note that $\bar{\tau}^{fail}$ is the average bond shear stress at joint failure. The load at joint failure, in Newtons, can be determined by simply multiplying $\bar{\tau}^{fail}$ by the bond's 14,900 mm^2 shear area.

As indicated in Table 1, one PMMA-to-aluminum joint (PMMA-1) was tested in compression, while the other PMMA-to-aluminum joint (PMMA-2) was tested in tension. In the compression test, the adhesive debonded stably under increasing load. Slow bond failure was observed visually at both ends of the joint test specimen, and strain gage data also reflect stable bond failure (Fig. 2). Bond failure initiated at the inner bond end where an aluminum adherend terminates and the PMMA adherend is fully loaded. The compressive strength listed in Table 1 for PMMA-1 corresponds to initial bond failure. The maximum compressive load reached during the test occurs when $\bar{\tau}$=0.8 MPa. At maximum load, the bond between one of the aluminum adherends and the PMMA adherend failed completely, and roughly 50% of the bond to the other aluminum adherend had also failed. In tension test PMMA-2, the PMMA adherend failed abruptly in the region where one of the aluminum adherends terminates. No bond failure was observed prior to the fracture of the PMMA adherend. The measured compressive strength of the PMMA-to-aluminum joint is less than 50% of its tensile strength.

Table 1. Test Results

TEST	JOINT	LOAD	$\bar{\tau}^{fail}$[1] (MPa)	FAILURE
PMMA-1	PMMA-ALUMINUM	COMPRESSIVE	0.6	BOND
PMMA-2	PMMA-ALUMINUM	TENSILE	1.9	PMMA
E/G-1	E-GLASS/ EPOXY-ALUMINUM	TENSILE	13.4	BOND
E/G-2	E-GLASS/ EPOXY-ALUMINUM	TENSILE	20.1	BOND

1 failure load/bond shear area

The E-glass/epoxy joints were both tested in tension. The two nominally identical joints have substantially different measured strengths. The average tensile joint strength corresponds to $\bar{\tau}$=16.8 MPa, with individual strengths of 80% and 120% of this average. These test results clearly illustrate that even when joints are carefully fabricated, there can be substantial variability in joint strength. Because of the opaque nature of the outer E-glass/epoxy adherend, the failure sequence in tests E/G-1 and E/G-2 cannot be established with complete certainty. Failure occurred abruptly in both tests with no preliminary load drops. Furthermore, strain gage data give no indication of bond failure prior to joint failure. In test E/G-1, the bond on one end of the joint test specimen failed

completely at maximum load. An ultrasonic evaluation of the bond on the other end of the joint test specimen showed no debonding. In test E/G-2, a partial bond failure occurred at one end of the joint test specimen. Bond failure is thought to have initiated at the inner bond end and run to the region of the fill holes drilled through the E-glass/epoxy adherend (~40 mm from the tube end, see the JOINT TEST SPECIMEN section above for a description of the fabrication method). The E-glass/epoxy adherend fractured on the plane defined by the four fill holes, thus allowing the aluminum adherend with a 40 mm portion of the E-glass/epoxy tube attached to slide relative to the rest of the joint. An ultrasonic evaluation of the bond on the other end of the joint test specimen indicates that 30% of that bond, in the region adjacent to the inner bond end, had failed. Since strain gage data give no indication of stable debonding, this partial bond failure may have occurred when the other end of the joint test specimen failed abruptly.

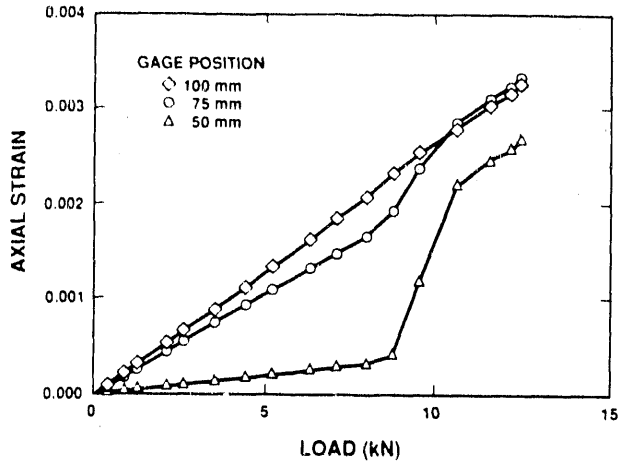

Fig. 2. Measured strains in test PMMA-1 reflect stable bond failure. Loads and strains are compressive and the gage position is measured relative to the end of the PMMA adherend.

All joint test specimens were instrumented with strain gages along the length of the outer adherend. Figure 3 plots strain gage results for tests PMMA-1 and PMMA-2, while Figure 4 plots results for tests E/G-1 and E/G-2. Note that 1) gage position is measured relative to the end of the outer adherend with bond ends at 0 and 75 mm, 2) measured strains are connected with straight line segments to approximate the strain distribution along the length of the outer adherend, 3) data for a load level of roughly 40% and 100% of the joint failure load are plotted for each test, and 4) plotted axial strains are normalized with respect to ε_0, the strain found at the specimen's midplane (where strains are uniform and unaffected by the adhesive bond). If a joint responds in a fully linear elastic manner, strain distributions normalized in this manner will show no load dependence. The normalized strain distributions for the PMMA-to-aluminum joints do suggest that the joint behaves in an essentially linear manner prior to failure, and strain distributions for the tensile and compression tests are indistinguishable (Fig. 3). The normalized strain distribution for test E/G-2, the most highly loaded E-glass/epoxy composite-to-aluminum joint, does seem to show some load dependence (Fig. 4). The axial strain distributions for the two different outer adherends are compared in Figure 5. These results indicate that load transfer from the inner aluminum adherend to the outer adherend is nonuniform, and that the relatively compliant PMMA adherend has the shorter load transfer length.

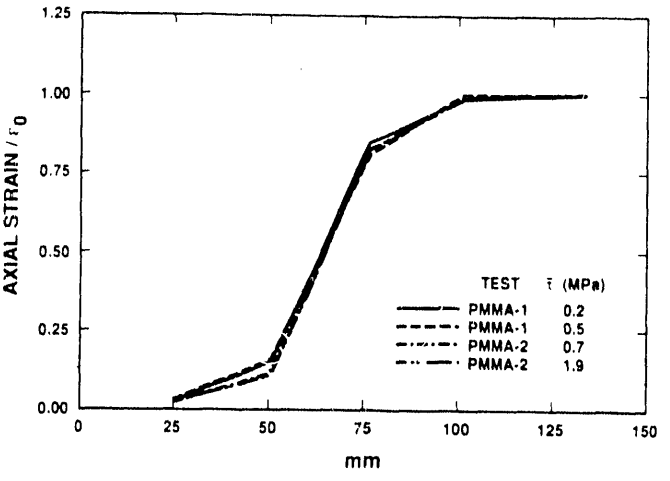

Fig. 3. Normalized strain distributions along the length of the outer adherend for tested PMMA-to-aluminum joints.

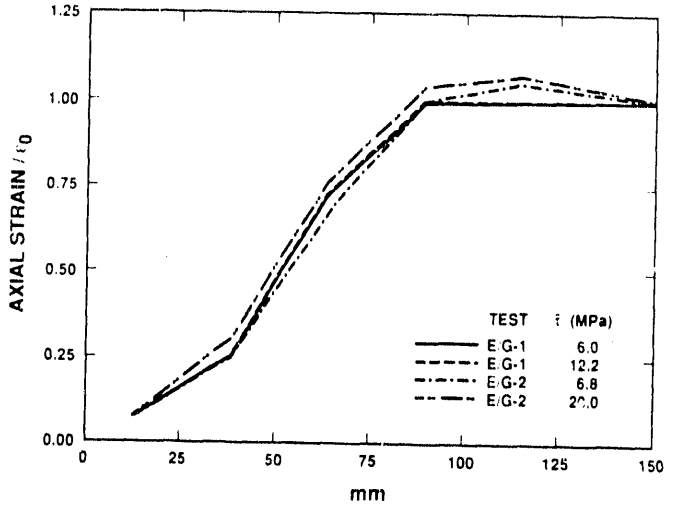

Fig. 4. Normalized strain distributions along the length of the outer adherend for tested E-glass/epoxy composite-to-aluminum joints.

ANALYSIS AND DISCUSSION

An axisymmetric, finite element analysis of the tested joints has been carried out using Version 4.7 of the ABAQUS finite element code [3]. The dimensions of the tubular joint geometry analyzed are listed in Figure 1, while the finite element mesh used in the analysis is shown in Figure 6. Since the joint is symmetric about its midplane, symmetry conditions are applied and only one half of the joint is analyzed. The joint is loaded by uniformly displacing the end of the aluminum adherend. The bond is modeled with four elements through its thickness, and the mesh is refined at the bond ends where the highest stress gradients are expected. This model contains 4150, 4- node, reduced integration, axisymmetric elements (CAX4R elements).

Since the adhesive bond was cured at room temperature, thus minimizing residual fabrication stresses, residual fabrication stresses are not considered in the present analysis.

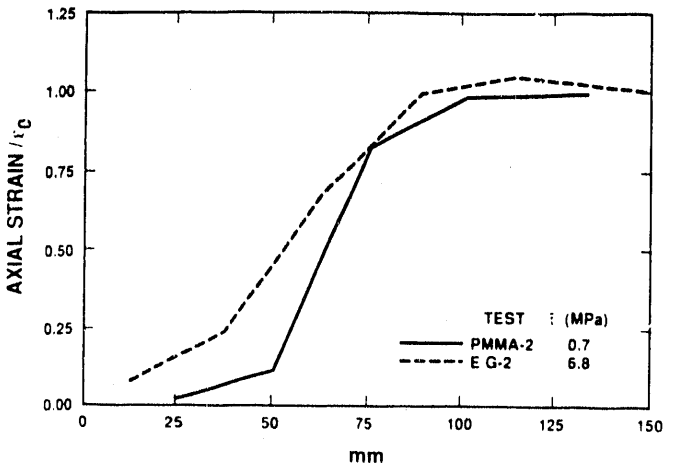

Fig. 5. Comparison of normalized strain distributions along the length of the outer adherend for PMMA and E-glass/epoxy outer adherends.

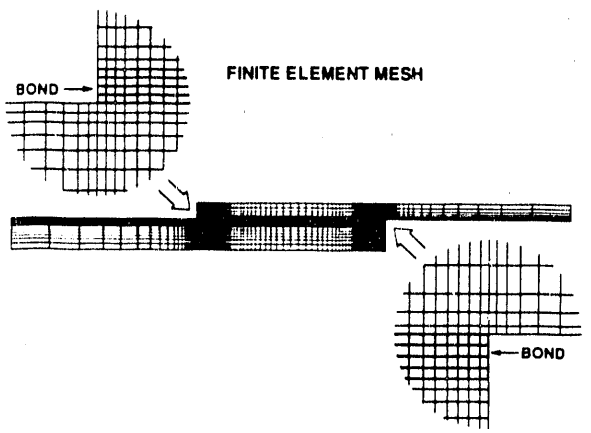

Fig. 6. Finite element mesh used to analyze tubular lap joints.

The aluminum inner adherend and the PMMA or E-glass/epoxy outer adherend are all modeled as linear elastic materials. The aluminum is considered to be isotropic with a Young's modulus of 69.5 GPa and a Poisson's ratio of 0.33. Likewise, the PMMA is considered to be isotropic with a Young's modulus of 2.75 GPa and a Poisson's ratio of 0.40. The E-glass/epoxy is modeled as an orthotropic material. An axial modulus of 22.5 GPa was measured during the joint test. An axial-to-hoop Poisson's ratio of 0.17 was also measured. Other E-glass/epoxy properties are estimated using known unidirectional properties and fabric construction. Specifically, the estimated radial and hoop Young's modulus are 10 GPa and 28 GPa, respectively, the estimated shear modulus is 5 GPA, and estimated radial-to-axial and radial-to-hoop Poisson's ratio are both 0.10. The Hysol EA 9394 paste adhesive used to bond the adherends together is modeled as an elastic-plastic material. Its tensile stress-strain relation is defined in Figure 7. Cast, dog-bone tensile specimens were used to measure the adhesive's initial stress-strain response, however, these specimen's contained voids that initiated premature failure. Therefore, the response at higher loads is simply estimated, with a maximum strength similar to other high strength adhesives.

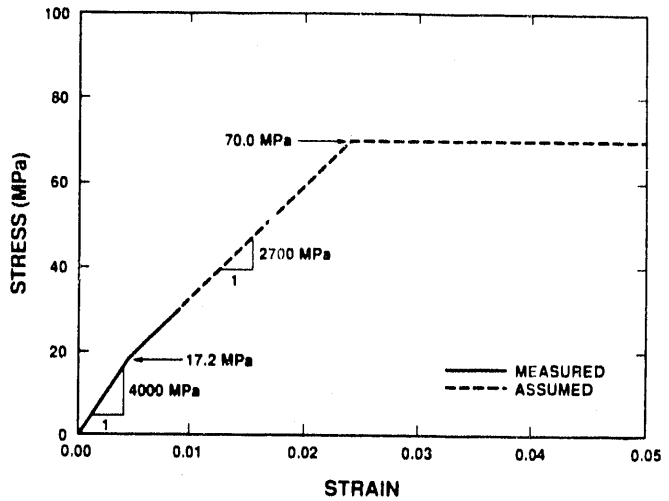

Fig. 7. Adhesive's tensile stress-strain relation used in finite element analysis.

Calculated nondimensional strain distributions along the outer PMMA adherend are plotted in Figure 8 for three different load levels. Since the analysis predicts little plastic yielding at a load level of $\bar{\tau}$=2.0 MPa (a load exceeding that observed in any PMMA-to-aluminum test), the nondimensionalized strain distributions for the three load levels overlay. Note that even though the bond terminates 75 mm from the end of the adherend, the axial strain becomes uniform only at distances greater than 100 mm. This is the result of tubular bending of the outer adherend in the region where the bond terminates. Measured strains from test PMMA-2 are also shown in Figure 8 for three similar load levels. These data points also overlay and analysis and experiment are in excellent agreement. This agreement lends some credence to calculated stresses.

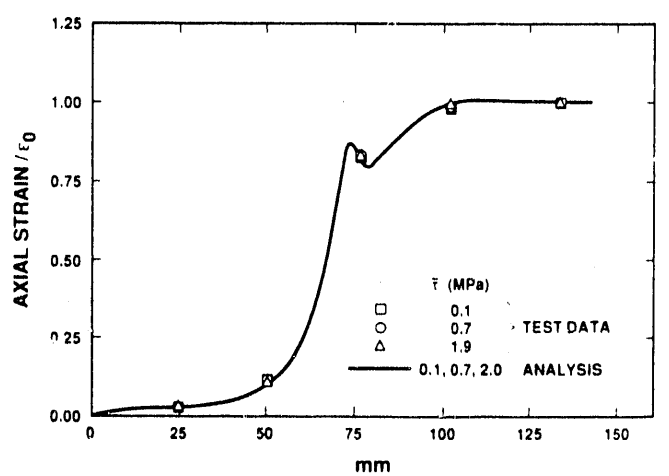

Fig. 8. Calculated normalized strain distribution along the length of the outer adherend of a PMMA-to-aluminum joint.

Figure 9 plots the calculated shear stress and Figure 10 the radial stress acting on the epoxy-to-PMMA interface for three load levels of interest. Calculated bond stresses in a lap joint are rather complex, and there are several factors that influence the nature of the stress distribution. Load is transferred from one adherend to the other by shear, and the shear stress distribution would be essentially uniform if the adherends were rigid. However, the adherends have finite stiffness, and this allows the axial strain in the adherends to differ. Differential adherend straining elevates shear stresses at the ends of the bond. Furthermore, differential straining is magnified when there is an imbalance in adherend stiffness, and shear strains are intensified at the bond end from which the less stiff adherend extends [4]. Since the adherend stiffness ratio for the PMMA-to-aluminum joint is 25, the calculated shear stress distributions in Figure 9 reflect the effect of substantial differential straining. Calculated shear stresses are substantially higher at the inner bond end where the PMMA adherend begins to fully carry the applied load (i.e. the bond end located 75 mm from the end of the PMMA outer adherend). The bond is also subjected to a radial or peel stress (Fig. 10). Poisson's ratio effects and tubular end-moments generated by bondline shear stress combine to create deformations that are resisted by peel stress. The magnitude of the calculated peel stresses is also greatest at the inner bond end. The calculated peel stress is compressive for an applied tensile load. This may explain why the bond failed in the compressive PMMA-1 test (calculated tensile peel stress), and not in the tensile PMMA-2 test (calculated compressive peel stress). It should be finally noted that, in the region where the bond terminates, over a distance of the order of the bond thickness, the shear stress quickly decays to satisfy a stress-free condition at the end of the bond. A very complex stress state exists in this region, and within the context of continuum mechanics, stress and strain singularities can exist at points where an interface intersects the free surface. Consequently, stresses calculated using standard finite element techniques cannot be considered reliable within roughly one adhesive thickness (0.25 mm) of the bond's end.

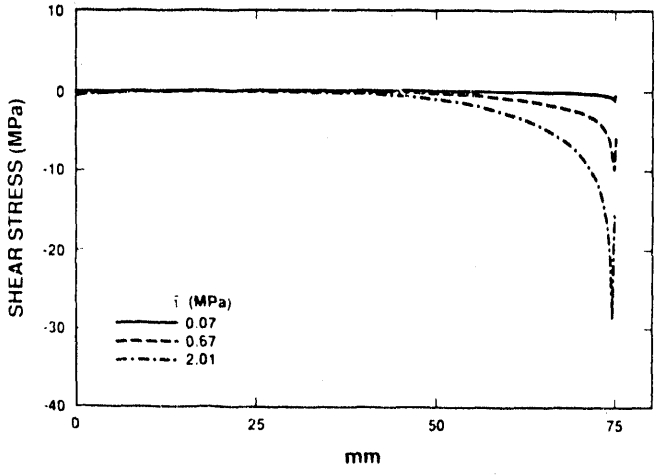

Fig. 9. Calculated shear stress distribution along the epoxy-to-PMMA interface. Distance measured relative to the end of the PMMA adherend.

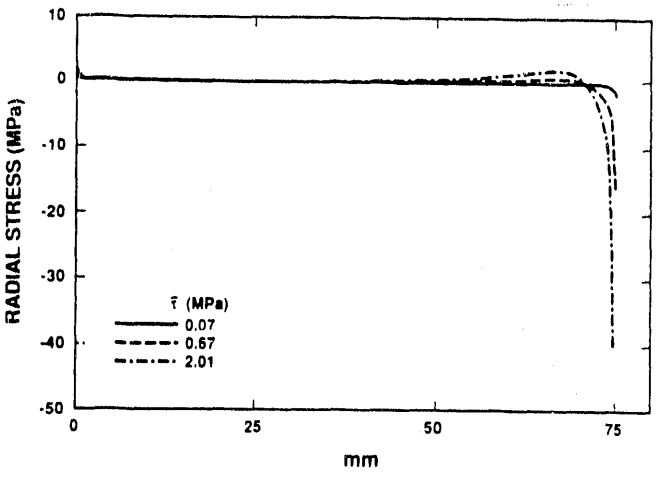

Fig. 10. Calculated radial stress distribution along the epoxy-to-PMMA interface.

The E-glass/epoxy composite-to-aluminum joint was also analyzed. Figure 11 plots the nondimensionalized strain distribution along the outer E-glass/epoxy adherend for three different load levels. Measured data for similar load levels are also plotted. The analysis indicates that extensive bond yielding occurs when loads exceed $\bar{\tau}$=10 MPa. Extensive bond yielding causes the calculated nondimensionalized strain distributions to shift with load. Nondimensionalized E/G-2 test data also show a shift with increasing load, and are in good agreement with calculated results. Figure 12 plots the calculated shear stress and Figure 13 the calculated radial stress along the epoxy-to-E-glass/epoxy interface for three load levels of interest. The shear stress distributions clearly show that there is large scale bond yielding as load increases. As discussed above, the presence of elevated shear stress and peel stress at bond ends is expected. Since the E-glass/epoxy composite-to-aluminum stiffness ratio is substantially lower than that of PMMA-to-aluminum (3 versus 25), calculated shear and peel stress distributions are not as highly biased to the bond end from which the loaded outer adherend extends.

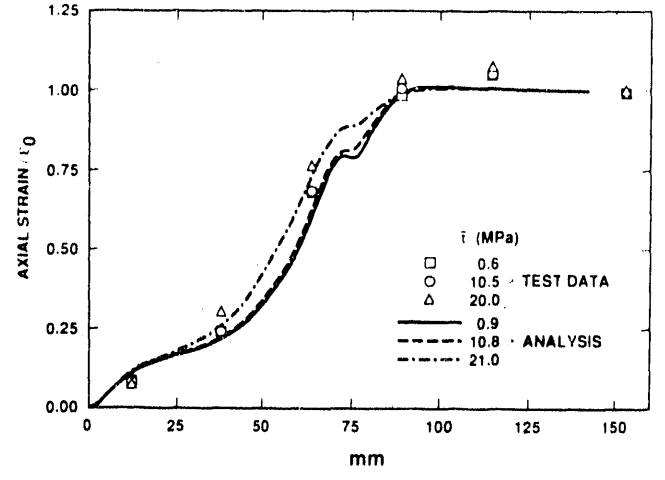

Fig. 11. Calculated normalized strain distribution along the length of the outer adherend of a E-glass/epoxy composite-to-aluminum joint.

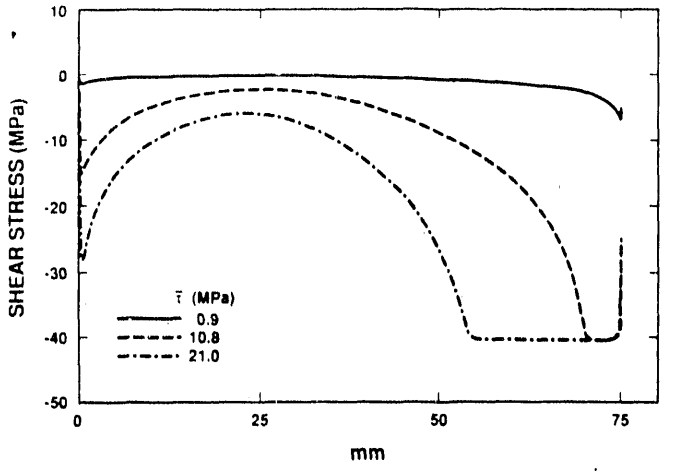

Fig. 12. Calculated shear stress distribution along the epoxy-to-E-glass/epoxy interface. Distance measured relative to the end of the E-glass/epoxy adherend.

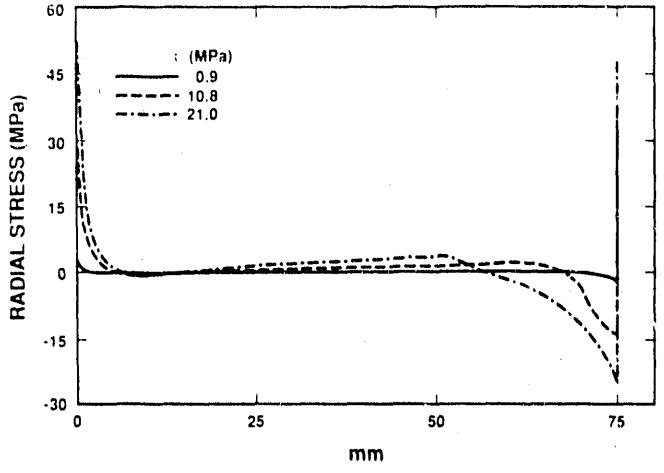

Fig. 13. Calculated radial stress distribution along the epoxy-to-E-glass/epoxy interface.

SUMMARY

Two PMMA-to-aluminum and two E-glass/epoxy composite-to-aluminum thick-walled, adhesively bonded, tubular lap joints have been loaded monotonically to failure. The measured compressive strength of the PMMA-to-aluminum joint is less than 50% of its measured tensile strength. In the compression test, adhesive bond failure occurred under increasing load, while in the tension test, the PMMA tube failed abruptly. The E-glass/epoxy composite-to-aluminum joints were both tested in tension. These joints failed abruptly when the adhesive bond failed. The two nominally identical joints failed at load levels that differed by 40%; a clear illustration of the variable nature of joint strength.

Strain gages, placed along the length of the thick outer adherend, were used to characterize load transfer between the adherends. The strain data indicate that load transfer from one adherend to the other is nonuniform, and that the relatively compliant PMMA adherend has the shorter load transfer length. The strain gage data also suggest that the PMMA-to-aluminum joint behaves in an essentially linear manner to failure, while the E-glass/epoxy composite-to-aluminum joint exhibits some material nonlinearity when highly loaded. A finite element analysis of the tested joints predicts strains that are in excellent agreement with those measured. The analysis indicates that bond stresses are highest in the region of observed failure, and that extensive bond yielding occurs when the E-glass/epoxy composite-to-aluminum joint is highly loaded.

ACKNOWLEDGMENTS

E. A. Correa developed procedures for fabricating tubular lap joints with a void-free, uniform thickness bond and also assembled all tested joints. M. E. Stavig strain-gaged the specimens and carried out the joint tests. He also carried out the tests on the neat EA 9394 adhesive. P. D. Walkington conducted the pre-test and post-test ultrasonic inspections of the joint specimens. This work performed at Sandia National Laboratories supported by U. S. Department of Energy under Contract DE-AC04-76DP00789.

REFERENCES

1. Lubkin, J. L., and Reissner, E., "Stress Distribution and Design Data for Adhesive Lap Joints Between Circular Tubes," Transactions of the ASME, Vol. 78 (1956), pp. 1213-1221.

2. Adams, R. D., and Peppiatt, N. A., "Stress Analysis of Adhesive Bonded Tubular Lap Joints," Journal of Adhesion, Vol. 9 (1977), pp. 1-18.

3. ABAQUS, Hibbitt, Karlsson, & Sorensen, Providence, Rhode Island.

4. Hart-Smith, L. J., "Designing Adhesive Bonds," Adhesives Age, October 1978, pp. 32-37.

END

DATE FILMED

12/04/90